The Supercritical Pile Model for GRBs

A. Mastichiadis

Department of Physics, University of Athens, Panepistimiopolis, GR 15783, Zografos, Greece

D. Kazanas

Laboratory for High Energy Astrophysics, NASA/GSFC, Code 661, Greenbelt, MD 20771

ABSTRACT

We present the spectral and temporal radiative signatures expected within the "Supercritical Pile" model of Gamma Ray Bursts (GRB). This model is motivated by the need for a process that provides the dissipation necessary in GRB and presents a well defined scheme for converting the energy stored in the relativistic protons of the Relativistic Blast Waves (RBW) associated with GRB into radiation; at the same time it leads to spectra which exhibit a peak in the burst νF_ν distribution at an energy $E_p \simeq 1$ MeV in the observer's frame, in agreement with observation and largely *independent* of the Lorentz factor Γ of the associated relativistic outflow. Futhermore, this scheme does not require (but does not preclude) acceleration of particles at the shock other than that provided by the isotropization of the flow bulk kinetic energy on the RBW frame. In the present paper we model in detail the evolution of protons, electrons and photons from a RBW to produce detailed spectra of the prompt GRB phase as a function of time from across a very broad range spanning roughly $4 \log_{10} \Gamma$ decades in frequency. The model spectra are in general agreement with observations and provide a means for the delineating of the model parameters through direct comparison with trends observed in GRB properties.

Subject headings: Gamma Ray Bursts: Radiation Mechanisms; Plasmas: Relativistic

1. Introduction

The discovery of GRB afterglows by BeppoSAX (Costa et al. 1997) and the ensuing determination of their redshifts (van Paradijs et al. 1997) by and large settled the issue of

their distance and luminosity. This discovery, then, settled also the issue of their energetics in favor of emission by Relativistic Blast Waves (RBW) moving toward the observer with Lorentz factors $\Gamma \sim 100 - 1000$, as it had been discussed earlier by Rees & Mészáros (1992) and Mészáros & Rees (1992). The relativistic boosting of the radiation emitted at the rest frame of the RBW (by $\simeq \Gamma^4$ in luminosity) then resolved also the issue of their huge energy budget requirements (if at cosmological distances) and brought them to agreement with the energy release in stellar gravitational collapse. At the same time it provided consistency between the huge implied GRB luminosities and their apparently thin spectra (Krolik & Pier 1991; Fenimore, Epstein & Ho 1993; Barring & Harding 1995). The same considerations provided also (Rees & Mészáros 1992) an order of magnitude relation between the GRB duration Δt and the size of the radiating region, namely $R \simeq 10^{16}(\Delta t/30 \text{ sec})\,(\Gamma/100)^2$ cm.

These estimates of the kinematic state of the GRB emitting plasma have been supplemented by certain dynamical considerations. For example, following the work of Shemi & Piran (1990) it has been generally accepted that a certain amount of baryons must be carried off with the blast waves responsible for the GRBs. This baryon contamination has even been deemed necessary for the efficient transport of the GRB energy away from the environs of its "inner engine", else the entire blast wave's internal energy would be converted into radiation on very short time scales, leading to events of very different temporal and spectral appearance (e.g. Paczyński 1986) than the observed GRB. In fact, the original models of Rees & Mészáros (1992) and Mészáros & Rees (1992) relied on the presence of a rather precise amount of baryons within the GRB fireball: enough to keep the fireball optically thick and thus allow the conversion of its internal energy to directed motion upon its expansion, but not too many as to render it only mildly (or even non-) relativistic. Even in the more recent (and perhaps more plausible) variants of the same model that use Poynting flux (rather than photon energy density) as the agent responsible for the RBW acceleration (see Vlahakis & Königl 2002, 2004), the circumstellar matter swept up by the RBW to the radius of $R \sim 10^{16}$ cm, contains roughly as much energy stored in protons as in magnetic field. In either case, the models are called to shed light to these two generic, still open, issues of the GRB dynamics: (a.) The acceleration of the associated Relativistic Blast Waves to Lorentz factors $\Gamma \sim 10^2 - 10^3$ (b.) The dissipation of the energy stored in protons and/or magnetic fields at the rates necessary to produce the prompt GRB emission with the proper attributes. Both these issues are still open in GRB physics.

An altogether different issue associated with the prompt GRB emission is that of their spectra. The differential photon GRB spectra can be fit very well by the so-called Band-spectrum (Band et al. 1993) that consists (asymptotically) of two power laws of indices α

and β joining smoothly at a break energy E_b, i.e.

$$N(E) \propto \begin{cases} E^\alpha \ e^{-(\alpha-\beta)E/E_b} & \text{for } E < E_b \\ E^\beta \ E_b^{\alpha-\beta} \ e^{-(\alpha-\beta)} & \text{for } E > E_b \end{cases} \tag{1}$$

It was pointed out by Malozzi et al. (1995), and confirmed by a larger sample of *BATSE* data (Preece et al. 2000), that the values of E_b are narrowly distributed around $E_b = 200$ keV with a similarly narrow distribution for α around the value $\alpha = -1$, while the distribution of β has a maximum near $\beta \simeq -2.3$ and extends to values $\beta \lesssim -4$, with only few bursts having $\beta > -2.3$. These values imply that the GRB peak energy of their νF_ν spectra, (i.e. the peak energy of their emitted luminosity $E_p = (\alpha + 2) E_b/(\alpha - \beta)$) is equally narrowly distributed about the same energy which, when corrected for the GRB redshift ($z_{\text{GRB}} \sim 1 - 2$), shifts close to $E_p \simeq 0.5$ MeV.

Both the presence of the narrowly distributed energy E_p and the value of the low energy index $\alpha \simeq -1$ are hard to understand within the conventional wisdom models which suggest that the observed prompt GRB $\gamma-$ray emission is due to synchrotron radiation by relativistic electrons. Under these assumptions, E_p should be proportional to Γ^4 (two powers of Γ come from the synchrotron emission, one from the magnetic field - assuming equipartition with the postshock matter, and one more from the transformation of this energy to the lab frame). This strong dependence on the value of Γ would imply a rather unique value for this latter parameter, else the E_p range would be much broader than observed, in disagreement with observation. While there may indeed be a reason for a very narrow range in the values of Γ consistent with the observed range of E_p, as of today such a reason is unknown (at least to the authors). If the same emission is due to electrons accelerated to energies beyond those implied by the shock Rankine - Hugoniot conditions (i.e. $\gamma_e \simeq \Gamma$), or to a low energy cut-off E_c in the electron injection spectrum (with $E_c \gg \Gamma m_e c^2$), the presence of a rather well defined peak in the GRB νF_ν spectra is even harder to understand, as in either case there is no apparent reason for such a well defined energy scale.

Considerations along similar lines do argue for very specific values for the low energy power law index α: If the observed peak in the νF_ν spectra is due to synchrotron emission by a $\delta-$function-like electron distribution, α should be that corresponding to the single electron synchrotron emissivity, $\alpha = -2/3$ (Katz 1994a), while if the observed peak is due to a low energy cut-off in the electron injection spectrum, the associated extremely fast cooling should lead to $\alpha = -3/2$ (Ghisellini 2002). The observed values extend outside the above range, while the most likely values are inconsistent with either of these assumptions in the context of synchrotron radiation for the prompt GRB emission.

The discovery of GRB afterglows, following the prediction by Katz (1994b) shifted attention from the prompt GRB phase to that of the afterglow. Novel issues related to the

physics of GRB ouflows have since emerged, e.g. the narrow range of the total GRB energy budget (Frail et al. 2001; Bloom et al. 2003) and the correlation of GRB luminosities with their spectral lags (Salmonson & Galama 2003). In general, the afterglows extended the frequency range of GRB study to the X-rays, optical, IR and radio thus greately expanding our means of probing of the RBW of GRB (see Zhang & Mészáros 2004; Piran 2004 for reviews). In the midst of this new flurry of activity, the issues of dissipation of the GRB proton kinetic energy and the narrow $E_{\rm p}$ distribution, while quietly ignored, have remained largely unanswered. One of the few attempts to address these issues was that of Kazanas, Georganopoulos & Mastichiadis (2002; hereafter KGM): In search of a well defined and tractable dissipation mechansim, they proposed a process that utilises proton - photon collisions to convert the energy stored in protons behind the forward shock of the RBW to electrons (and then into radiation). KGM provided the kinematic and dynamic thresholds for this process to take place and showed that, in addition, it produced spectra that peaked at several well defined energies, namely at $\sim 2m_e c^2/\Gamma^2$, $2m_e c^2$, $m_e c^2 \Gamma^2$, *in the observer's frame*. The interesting feature of this model is that the combination of the threshold for pair production energy and the final Lorentz boost to the observer's frame leads to a spectral peak at $\sim m_e c^2$ *largely independent* of the Lorentz factor Γ of the RBW, provided that the latter is larger than a threshold value which depends on the value of the magentic field of the RBW. Therefore, the process described by KGM provides a framework for resolving both the proton-to-electron-energy-transfer and the narrow E_p–range problems in a single fell swoop. Besides the above properties, this model differs from most in the present literature in several respects: (a) It does not require (but does not preclude either) the presence of accelerated particle populations, other than those produced by the isotropization of the RWB kinetic energy behind the shock. (b) It does not require equipartition between the proton and electron enery densities. (c) It posits that the observed radiation in the X - γ ray band is upscattered (and then blue-shifted) synchrotron radiation rather than simply blue-shifted synchrotron radiation.

The purpose of the present paper is to present detailed calculations based on the model outlined in KGM, which for reasons explained below (and in the original reference), is referred to as the "Supercritical Pile" model for GRB. In §2 of this note we provide a qualitative description of the basic notions that underlie the "Supercritical Pile" model and how they apply to GRB. In §3 we describe the details of the model and of the numerical method employed for the solution. In §4 we describe the numerical tests used in making certain that our results make sense and the code works as planned in the case that contains no electrons but produces all necessary electrons from the proton radiative instability. In §5 we repeat the calculations of §4 in the more realistic case that includes also the effects of the presence of electrons. We also present light curves and spectra produced within the model for different

values of the relevant parameters. Finally in §6 the resuts are summarised and conclusions are drawn.

2. Dissipation: The Proton-Pair-Synchrotron (PPS) Network

The name of our model derives from the (at first sight incredulous) similarity between the RBW of a GRB and a nuclear pile. However, a closer inspection - albeit with our model in mind - reveals the following similarities: (a) They both contain a large amount of free energy, stored in relativistic protons in the GRB case and in nuclear binding energy in the case of the pile. (b) This energy can be released explosively - i.e. on the time scale of crossing the relevant size by photons or neutrons respectively, once identical criticality conditions are met. Furthermore, besides the possibility of the explosive release of the energy contained in the relativistic protons of a RBW, our model also provides an account for the observed peak in the νF_ν GRB spectra; interestingly it achieves this in one of its variants conceived to provide agreement between the numerical values of the parameters that determine the criticality condition with those associated with the GRB settings. It is interesting to note that processes involving the exponential increase of the number of photons or their luminosity akin to the criticality condition of a nuclear pile discussed above and in the rest of this paper are not new in astrophysics; we are aware of two such instances, one involving the energy released through the comptonization of soft photons by hot electrons (Katz 1976) while the other the equilibration of plasmas through the Double Compton process (Lightman 1981).

The process we model in detail in the following has two distinct aspects, along the lines of the two GRB issues discussed above. The first one concerns the transfer of the energy stored in a population of relativistic hadrons (protons) into leptons. This has been discussed originally by Kirk & Mastichiadis (1992; KM92) and modeled in more detail in Mastichiadis & Kirk (1995; MK95) and Mastichiadis, Protheroe & Kirk (2005; MPK05). This same process was then modified to include the effects of relativistic motion of the plasma in the possibility that some of its photons could be scattered by matter (a "mirror") located upstream along the direction of motion. This leads to a relaxation of the threshold conditions obtained in KM92 and was discussed by Kazanas & Mastichiadis (1999; KM99). The second aspect concerns the spectra that result from the combination of these processes as was originally discussed in KGM and their relation to the energetics of GRB.

To formulate the conversion of proton energy to leptons through the $p\gamma \rightarrow p e^+ e^-$ process one assumes the presence of a population of relativistic protons of the form $N(\gamma_p) = n_0 \gamma_p^{-\beta}$; the requisite photons are provided by the synchrotron radiation of the pairs produced in the proton - photon intereactions, with these two processes combined into a reaction

network. This network involves both kinematic and dynamic thresholds. The physical arguments that provide these thresholds are rather simple: There is a *kinematic* threshold for the reaction $p\gamma \rightarrow pe^+e^-$; for a photon of energy E_γ, there is a critical value $\gamma_c = 2m_ec^2/E_\gamma$ of the proton Lorentz factor for the reaction to take place (assuming a head-on photon-proton collision, else this condition should involve the cosine of the angle between these particles), with each lepton produced by this reaction with energy $\gamma_c\, m_ec^2$ (on the average). The reaction network will be *self-contained* if these pairs can produce, through the synchrotron process, the photons needed to effect the pair production, i.e. if $E_\gamma = E_s = b\,\gamma_c^2\,m_ec^2$ (b is the magnetic field B of the plasma in units of the critical magnetic field $B_c = m_e^2\,c^3/c\hbar = 4.4\ 10^{13}$ G). This leads to the following kinematic threshold for the reaction network $\gamma_c^3\,b \simeq 2$ or $\gamma \simeq (2/b)^{1/3}$, as discussed in KM92.

The combined network of the photon and pair producing reactions will also be *self-sustained* if *at least one* of the synchrotron photons produced by the $e^+\,e^-$ pairs produces another pair before escaping the volume of the plasma in a reaction with a sufficiently energetic proton (i.e. one that fulfills the kinematic threshold). This results in a condition for the column density of the plasma which is identical to that of a critical nuclear chain reaction (we re-iterate for the benefit of the reader that criticality is a condition on the column density rather than the - erroneously referred to in the popular literature - mass of the pile). Therefore, the plasma column density (at the proton critical energy), must be greater than the inverse of the number of synchrotron photons emitted by the electrons of Lorentz factor γ_c. The number of synchrotron photons just above the threshold energy is $\mathcal{N} = \gamma_c/b\,\gamma_c^2 = 1/b\,\gamma_c$ leading to the dynamic condition $\tau_{p\gamma} \simeq \sigma_{p\gamma}\,R\,N_p(\gamma_c)\,\gamma_c \gtrsim b\,\gamma_c$. Taking into account the kinematic threshold condition this reads $\sigma_{p\gamma}\,R\,n_0 \gtrsim b^{(1-\beta/3)}$, in agreement with the result of KM92.

Mastichiadis & Kirk (1995) and Mastichiadis, Protheroe & Kirk (2005) have explored the above process numerically in detail and found the semianalytic estimates above to be in excellent agreement with the more detailed numerical studies. The instability depends on both thresholds as described and converts the energy density stored in relativistic protons (those with energy above that of the threshold $\gamma_p \geq \gamma_c$) into pairs on the plasma crossing time scale R/c. During the initial (linear) regime of the instability the pair and photon numbers increase exponentially ($\propto e^{st}$) with the exponent s being greater the larger the value of the proton density n_0 (i.e. the farther the network is above threshold), while $s = 0$ at precisely the threshold value of this parameter.

The RBW associated with the GRB provide a natural setting for the production of relativistic proton populations, thus lending them as natural sites where the above considerations should apply. However, relativistic motion alone does not in general change the kinematic

and dynamic threshold conditions obtained above. It is conceivable that the presence of a relativistic proton population that extends to sufficiently high energies could satisfy the kinematic threshold of the instability; however, the "standard" GRB model parameters yield column densities for the relativistic protons (these are just those in the matter "swept-up" by the RBW) far smaller than necessary to satisfy the dynamical threshold condition.

As pointed out in Kazanas & Mastichiadis (1999; KM99) the situation can change drastically in the presence of matter along the direction of relativistic motion which could isotropize through scattering the radiation emitted by the relativistically moving plasma. In this case, the RBW can "catch-up" with the scattered photons which, when re-intercepted by the RBW, appear on its rest frame blue-shifted by a factor $4\Gamma^2$. If those were the synchrotron photons of energy $\epsilon_s \simeq b\gamma^2$ they will now have an energy $\epsilon'_s \simeq 4b\gamma^2\Gamma^2$ (in units of $m_e c^2$). Therefore, the kinematic condition for the *reflected* photons to produce e^+e^--pairs gets modified to

$$\gamma\,\epsilon'_s \gtrsim 2 \quad \text{or} \quad 2b\,\gamma^3\,\Gamma^2 \gtrsim 1. \tag{2}$$

Making the further restrictive assumption that the only relativistic protons are those which are produced by the isotropization of the swept-up matter by the RBW, we can set $\gamma = \Gamma$ to obtain the kinematic threshold condition

$$\Gamma^5 b \gtrsim 2 \quad \text{or} \quad \Gamma \gtrsim \left(\frac{1}{2b}\right)^{1/5}. \tag{3}$$

One can employ the same considerations used above to obtain the dynamical threshold of the instability in this case too. The number of photons produced by an electron of Lorentz factor Γ on the RBW will now be $\mathcal{N} \simeq \Gamma/b\,\Gamma^2 = 1/b\,\Gamma$; assuming that a fraction τ_{mir} of these photons are scattered by the mirror (and are therefore re-intercepted by the RBW) leads to

$$\sigma_{p\gamma}\,R\,n \gtrsim \frac{b\,\Gamma}{\tau_{\mathrm{mir}}} \quad \text{or} \quad 2\tau_{\mathrm{mir}}\,\sigma_{p\gamma}\,R\,n\,\Gamma^4 \gtrsim 1 \tag{4}$$

with the latter expression obtained from the former with the use of the kinematic threshold condition (we would like to thank P. Mészáros for pointing our an error in an earlier version of the above expression). Here $\sigma_{p\gamma}$ is the photopair (Bethe-Heitler) cross section as given by Motz et al. (1969). The quantity n above now denotes the value of the ambient density (one should note that the column density is a Lorentz invariant so that its value as given above is identical to its value on the RBW rest frame). This condition can be satisfied for values of the GRB parameters $n \simeq 10^3\,n_3$ cm^{-3} and $R = 10^{16}\,R_{16}$ cm for values of $\Gamma \gtrsim 100\,(n_3 R_{16})^{-1/4}$ (assuming $\tau_{\mathrm{mir}} \simeq 1$; see also discussion in §6).

3. Particle evolution and radiation: The kinetic equation approach

Having outlined the qualitative aspects of the 'Supercritial Pile' model we proceed to describe in detail the procedure used in simulating this model. We consider a Relativistic Blast Wave (RBW) moving with speed $v_0 = \beta_\Gamma c$, where $\beta_\Gamma = (1 - \Gamma^{-2})^{-1/2}$ and Γ the bulk Lorentz factor of the flow which we assume to be constant. It has a radius $R_{RBW}(t)$ as measured from the origin of our coordinate system (assumed to be the center of the original explosion) and it contains protons and electrons. If there is no particle acceleration taking place we can, conservatively, assume that both species have been isotropized and that in the flow rest frame they have distributions with average Lorentz factors $\langle \gamma_p \rangle \simeq \langle \gamma_e \rangle \simeq \Gamma$. Under these conditions, protons carry a significant fraction of the blast wave energy. The electron and proton distributions will evolve in time on the RBW frame since both species will suffer from various types of energy losses, physical escape, etc. At the same time they will radiate by synchrotron, inverse Compton and possibly other processes.

We assume also the presence of scattering material (which we will call the "mirror") ahead of the advancing shock. This is located between radii $R_{s,1}$ and $R_{s,2}$ and it is assumed to have a uniform electron density n_e^{sc} and a corresponding Thomson optical depth $\tau_{mir} = n_e^{sc} \sigma_T (R_{s,2} - R_{s,1})$ (at present, we consider only Thomson scattering as the main process that deflects the RBW synchrotron photons; other possibly important processes are at this stage ignored). Therefore part of the radiation emitted from the particles in the RBW will be intercepted by this mirror and scattered back, reentering the shock at a later time when this will have moved to a different location. The reflected (and amplified in energy) photons will contribute to the particles' (protons and electrons) energy losses, an additional feature of the present problem.

To treat the radiative transfer we assume that the relativistic blast wave is expanding in a spherical fashion, however, due to relativistic beaming an observer receives the radiation coming mainly from a small section of it of lateral width R_{RBW}/Γ and longitudinal width R_{RBW}/Γ^2 in the lab frame but R_{RBW}/Γ on the flow frame. Therefore, at the RBW frame, one can approximate the emitting region by a spherical 'blob' of radius $R_b = R_{RBW}/\Gamma$ and solve the radiative transfer problem for that region. The particles in the other segments of the blast wave may follow a similar evolution, however the radiation coming from them will not be observed at the Earth as it is beamed away from us at angles $> \Gamma^{-1}$, neither will be intercepted, for the same reason, by the segment in consideration and it will not affect the evolution of the particle distribution in it.

Alternatively we can assume, instead of a sphere, a segment of opening angle Θ. Our analysis does not change apart from the fact that the Doppler factor $\delta = [\Gamma(1 - \beta cos\theta)]^{-1}$ should be introduced when making the transformation of the radiation patterns betwwen

the RBW (comoving) and Earth (stationary) frames.

The problem of particle evolution in a homogeneous source region containing protons, electrons and photons was formulated and solved numerically by Mastichiadis & Kirk (1995) and more recently by Mastichiadis, Protheroe & Kirk (2005) adopting the kinetic equation approach. Herein we follow the same method, making the changes which are appropriate for the present case. The equations to be solved can be written in generic form

$$\frac{\partial n_i}{\partial t} + L_i + Q_i = 0 \tag{5}$$

where the index i can be any one of the subscripts 'p', 'e' or 'γ' referring to protons, electrons or photons respectively. The operators L_i denote losses and escape from the system while Q_i denote injection and source terms. These will be defined further below.

The unknown functions n_i are the differential number densities of the three species and the physical processes to be included in the kinetic equations are:

1. Proton-photon (Bethe-Heitler) pair production which acts as a loss term for the protons (L_p^{BH}) and an injection term for the electrons (Q_e^{BH})

2. Photopion production which also acts as a loss term for the protons (L_p^{π}) and and an injection term for both electrons (Q_e^{π}) and photons (Q_γ^{pi}).

3. Synchrotron radiation which acts as an energy loss term for electrons (L_e^{syn}) and as a source term for photons (Q_γ^{syn})

4. Synchrotron self absorption which acts as an absorption term for photons (L_γ^{ssa})

5. Inverse Compton scattering (in both the Thomson and Klein-Nishina regimes) which acts as an energy loss term for electrons (L_e^{ics}) and as a source term for high energy photons and a loss term for low energy photons, both effects included in Q_γ^{ics}

6. Photon-photon pair production which acts as an injection term for electrons ($Q_e^{\gamma\gamma}$) and as an absorption term for photons ($L_\gamma^{\gamma\gamma}$)

7. Electron-positron annihilation which acts as a sink term for electrons (L_e^{ann}) and as a source term for photons (Q_γ^{ann})

8. Compton scattering of radiation on the cool pairs, which impede the free escape of photons from the system.

A feature that differentiates our present study from MK95 and MPK05 is that processes involving photons in the left hand side (i.e. processes 1, 2, 5 and 6) can take place either with photons produced directly or with the photons which have been reflected by the mirror assumed to exist in front of the advancing shock.

In order to calculate the reflected photon number density as seen in the rest frame of the blob we use Eqn. (2) of Böttcher and Dermer (1998) corrected for Klein-Nishina effects. The reflected photon number density when the blob is at some distance z from the center is given by

$$n_\gamma^R(s_2, z_2) = \frac{3n_e^{sc}\sigma_T}{8c} \int_{\mu_2^{min}}^{\mu_2^{max}} d\mu_2 \int_{x_2^{min}}^{x_2^{max}} dx_2 D_1^2 \frac{\dot{N}(s_1, \Omega_1; z_1)}{x_1^2}(1 + cos^2\chi) \tag{6}$$

where s_1 and s_2 are the photon energies before and after reflection, z_1 and z_2 are the RBW spatial coordinate along the direction of motion at the instance of photon emission and reception, x_1 and x_2 are the distances of the reflection point from the RBW while this is at distances z_1 and z_2 respectively, μ_1 and μ_2 are the cosines of the angles that x_1 and x_2 make with the axis z, while χ is the scattering angle in the RBW. The energies of the photons before and after reflection are related by $s_1 = s_2/(D_1 D_2)$, where $D_1 = [\Gamma(1 - \beta_\Gamma\mu_1)]^{-1}$, $D_2 = \Gamma(1 - \beta_\Gamma\mu_2)$. The light travel-time effects are of great importance in our calculations. The causality condition

$$z_1 = z_2 - \beta_\Gamma(x_1 + x_2) \tag{7}$$

along with the condition $z_1 > 0$ implies that the blob does not receive any reflected photons for as long as it is at

$$z < z_{crit} = R_{s,1}\frac{2\beta_\Gamma}{1 + \beta_\Gamma}. \tag{8}$$

Therefore, if we assume for simplicity, that the RBW has reached a constant Lorentz factor Γ when it is some distance z_0 from the origin, then we can relate the current position of the RBW, z, with the time elapsed since then by the relation

$$z = z_0 + \beta_\Gamma ct. \tag{9}$$

With this hypothesis we can define a time

$$t_{crit} = \frac{z_{crit}}{\beta_\Gamma c} \tag{10}$$

with the property that only when $t > t_{crit}$, photons produced at earlier times will be reentering, due to reflection, the RBW.

A second point is that from the processes listed above photopion production, electron-positron annihilation, and Compton downscattering turn out to be totally unimportant for the parameters of the cases we will examine here. Photon-photon pair production also turns out to be of marginal importance. So, despite the fact that we keep all the aforementioned processes in the code, our focus is on the processes that provide the driving terms in the proton loop, i.e. the Bethe Heitler pair production (the source of pairs) [1], the electron synchrotron (the source of photons)[4] and inverse Compton scattering (the photon energization process)[5]. Further discussion on these points will be given in the last section.

With the inclusion of the leading terms only, the kinetic equations for each species read

- Protons

$$\frac{\partial n_{\mathrm{p}}}{\partial t} + L_{\mathrm{p}}^{\mathrm{BH}} + H(t - t_{\mathrm{crit}})L_{\mathrm{p}}^{\mathrm{BH,R}} = 0 \tag{11}$$

- Electrons

$$\frac{\partial n_{\mathrm{e}}}{\partial t} + L_{\mathrm{e}}^{\mathrm{syn}} + L_{\mathrm{e}}^{\mathrm{ics}} + H(t - t_{\mathrm{crit}})L_{\mathrm{e}}^{\mathrm{ics,R}} = Q_{\mathrm{e}}^{\mathrm{BH}} + H(t - t_{\mathrm{crit}})Q_{\mathrm{e}}^{\mathrm{BH,R}} + Q_{e}^{\gamma\gamma} + H(t - t_{\mathrm{crit}})Q_{e}^{\gamma\gamma,R} \tag{12}$$

- Photons

$$\frac{\partial n_{\gamma}}{\partial t} + \frac{n_{\gamma}}{t_{\mathrm{cr}}} + L_{\gamma}^{\gamma\gamma} + L_{\gamma}^{\mathrm{ssa}} = Q_{\gamma}^{\mathrm{syn}} + Q_{\gamma}^{\mathrm{ics}} + H(t - t_{\mathrm{crit}})Q_{\gamma}^{\mathrm{ics,R}} \tag{13}$$

We repeat here some of the comments made in MPK05 regarding these equations:

1. When the various terms above are written explicitly, equations (11), (12) and (13) form a non-linear system of coupled partial integrodifferential equations which are solved numerically.

2. The various rates are written in a manner that conserves power in the exchanges between the species.

3. Without the proton and reflection terms the system becomes identical to those considered in the 'one-zone' time-dependent leptonic models – see for example Mastichiadis & Kirk (1997).

We note however that the system of the equations is not identical to the one solved in MPK05:

4. The reflected photon number density which is computed by means of Equation (2) of Böttcher & Dermer (1998) depends on $n_{\gamma}(x, t')$ at all previous times (i.e. $t' < t$). Thus

no extra equation is required for this component. The function $H(t - t_{\text{crit}})$ is the Heaviside function denoting that the reflected photons start playing a role for $t > t_{\text{crit}}$, i.e. when the position of the RBW is inside the reflected photon zone –see Eqn. (6). Therefore at this point retardation effects become important.

3.1. Computational Details

The unknown functions n_i in Eqns (5)-(7) are the differential number densities of the three species, which are normalised as follows:

$$\text{Protons:} \quad \tilde{n}_{\text{p}}(\gamma_{\text{p}}, t)d\gamma_{\text{p}} = \sigma_{\text{T}}Rn_{\text{p}}(E_p, t)dE_p \quad \text{with } \gamma_{\text{p}} = \frac{E_p}{m_{\text{p}}c^2} \tag{14}$$

$$\text{Electrons:} \quad \tilde{n}_{\text{e}}(\gamma_{\text{e}}, t)d\gamma_{\text{e}} = \sigma_{\text{T}}Rn_{\text{e}}(E_e, t)dE_e \quad \text{with } \gamma_{\text{e}} = \frac{E_e}{m_{\text{e}}c^2} \tag{15}$$

$$\text{Photons:} \quad \tilde{n}_{\gamma}(x, t)dx = \sigma_{\text{T}}Rn_{\gamma}(\epsilon_{\gamma}, t)d\epsilon_{\gamma} \quad \text{with } x = \frac{\epsilon_{\gamma}}{m_{\text{e}}c^2} \tag{16}$$

and the time t has been normalised in all equations to the light-crossing time of the source $t_{\text{cr}} = R_b/c$.

With this definition the photon compactness becomes (we drop now the tilde for convenience)

$$\ell_{\gamma} = \frac{1}{3} \int dx x \frac{n_{\gamma}(x, t)}{t_{\text{cr}}} \tag{17}$$

while the compactness of the reflected photons can be defined in an analogous fashion

$$\ell_{\gamma}^R = \frac{1}{3} \int dx x \frac{n_{\gamma}^R(x, t)}{t_{\text{cr}}}. \tag{18}$$

Also the Thomson optical depth of the cooled electrons inside the blob is given by

$$\tau_{\text{T}}(t) = \int d\gamma \, n_{\text{e}}(\gamma = 1, t) \tag{19}$$

Finally, we can define the magnetic compactness

$$\ell_{\text{b}} = \sigma_{\text{T}}R\frac{B^2}{8\pi m_{\text{e}}c^2}. \tag{20}$$

For $\ell_{\text{b}} > max(\ell_{\gamma}, \ell_{\gamma}^R)$ the electron cooling is controlled by synchrotron while in the opposite case by inverse Compton scattering.

We note that the treatment of synchrotron and inverse Compton scattering has been improved over that described by MK95 in that the full emissivities are incorporated, rather than delta-function approximations. On the other hand, the Bethe-Heitler pair production still uses the delta-function approximation for the resulting electron-positron spectra. However, as shown in Mastichiadis, Protheroe, Kirk (2005; MKP05), this approximation does not alter the main results of KM92, MK95 or those of the present study.

4.   Modeling the PPS Network - No Electrons Present

Numerical studies of the proton loops in the absence of reflection have been presented already in MK95 and MPK05. For the clearer understanding of the effects and modifications caused by the presence of reflection we present in this section a similar numerical study taking reflection into account. As discussed in KM92, MPK05 and in Section 2 of the present paper, a relativistic proton distribution becomes unstable to the Proton-Pair-Synchrotron (henceforth PPS) loop if the two threshold conditions outlined there are satisfied (see relations (3, 4) of Section 2). This instability manifests itself with a spontaneous photon-pair growth characterised by an exponential rise in their respective densities of the form $n_\gamma \sim n_e \sim e^{st}$, with s being a function of both the number density and maximum energy of the protons. A second characteristic is that the maximum spectral luminosity of the produced photons occurs, at least during the initial stages of the instability growth, at the critical synchrotron frequency of the produced electrons. In this section we perform a numerical analysis using the code described in section 3 to explore the various characteristics of the PPS+reflection (henceforth PPSR) loop. In this approach we shall ignore, for the moment, the presence of any electrons in our initial conditions and focus only on the protons.

We consider, thus, that the RBW has a radius $R_{\text{RBW}} = 3.10^{16}$ cm $= R_{s,1}$ while it is cruising with a constant value of $\Gamma = 10^{2.6} \simeq 400$. According to the arguments presented in Section 3, with a good approximation one can consider the radiative transfer problem for only a segment of the RBW which we take it to be, for convenience, spherical with a radius $R_b = R_{\text{RBW}}/\Gamma = 7.5 \ 10^{13}$ cm. We assume that in this spherical blob there is a monoenergetic proton distribution with Lorentz factor $\gamma_p = \Gamma = 10^{2.6}$ and a number density $n_p = 10^4$ cm^{-3}. In the blob there is also a magnetic field of strength $B = 44$ Gauss, which was chosen arbitrarily, but in a way as to satisfy the threhold condition (Eqn. 2). We also assume that ahead of the expanding RBW there is a "mirror" of scattering material with total optical thickness $\tau_{\text{mir}} = 1$, distributed uniformly over its entire thickness. We apply the numerical code in a continuous run covering two distinct time intervals: (1) when the blob is still out of the reflection region ($t \leq t_{\text{crit}}$–Zone I) and (2) after it has entered this

region ($t > t_{crit}$–Zone II). The beginning of the run ($t = 0$) is set by the arbitrary requirement that 10 blob crossing times (as measured in the RBW frame) will elapse before the RBW reaches z_{crit}, the location where the reflected photons start entering the blob. Since we have restricted these set of runs to initial conditions for which there are initially no photons or energetic electrons within the plasma volume we consider, the time history of the blob in Zone I is irrelevant.

(i) The Growth Phase

As long as the RBW is in Zone I the protons do not suffer any substantial losses; therefore at the time the blob reaches z_{crit} it contains the original proton distribution while, according to our present assumptions, there are virtually no electrons or any other sources of photons. However, when it enters Zone II, depending on the proton parameters, the PPSR loop will begin operating. The parameters given above were chosen in such a way as to fulfill the required conditions. Figure 1 shows the spectrum at five consecutive crossing times as seen by an observer at rest in the RBW frame. He/she will observe the directly produced photons to grow with a spectrum which is peaked at an energy of about $\epsilon_s \simeq b\Gamma^2 = 1.6 \ 10^{-7}$ ($m_e c^2$ units), the characteristic synchrotron energy of electrons of Lorentz factor $\gamma_e = 398$ in a magnetic field of (normalized) strength $b = B/B_{cr} = 10^{-12}$ (for a discussion of these normalised units see Mastichiadis 2002). The photons in this case grow exponentially with index $s \simeq 5.1$. The reflected photons (represented by the dotted lines in this Figure) will be perceived in the RBW frame as having a much higher energy density than the directly produced internal photons, as they are amplified approximately by the factor $\alpha\Gamma^3$, where α is the albedo, while the maximum of their emission will occur at $\epsilon_{\mathcal{R}} \sim \Gamma^2 \epsilon_s \simeq b\Gamma^4 \simeq 3 \ 10^{-2} \ m_e c^2$. The reflected photons will cause additional cooling of the electrons by inverse Compton scattering as the magnetic compactness ℓ_b remains constant while the reflected photon compactness (ℓ_γ^R) increases with time – for all practical purposes cooling on the internally produced photons can be ignored as $\ell_\gamma \ll \ell_\gamma^R$). As a result of the inverse Compton cooling, the produced pairs will radiate an increasing fraction of their energy by this mechanism. Thus, the photon spectrum will consist of two components, the synchroton one at low energies and the ICS component at higher ones. As the interactions between the hot electrons and reflected photons will occur mostly in the Klein-Nishina regime (since $\gamma_e \epsilon_{\mathcal{R}} \sim b\Gamma^5 \simeq 10 \ m_e c^2$), the peak of this component will occur close to Γ. It is interesting to note that while the synchrotron component rises as e^{st}, the IC component rises like e^{2st} (since it depends on electons and photons which both rise like e^{st}). In this respect this process resembles the SSC process, with the crucial differences that in our present case the target photons are not the internally produced synchrotron photons but the reflected ones and the prime movers are protons, not electrons. The behaviour described can be seen in Fig. 1. Note that the IC component is not reflected at the "mirror" as the photons of this component appear in the

mirror rest frame with energies that are well within the KN regime and therefore kinematic effects do not allow the reflection of this component.
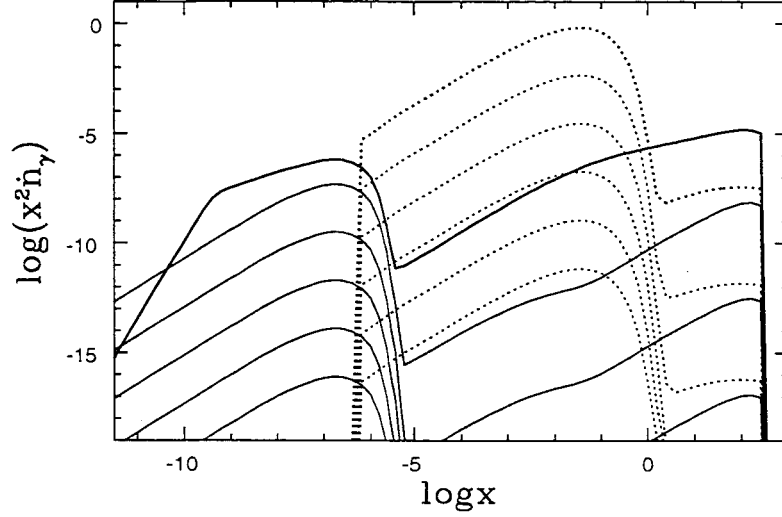

Fig. 1.— Snapshots, at consecutive crossing times, of the photon spectra (in code normalised units) during outgrowth as appear in the RBW frame. Here $\Gamma = 400$, $n_p = 10^4$ cm^{-3}, B=44 G (comoving values) and $\tau_{\mathrm{mir}} = 1$. Photon energy is expressed in $m_e c^2$ units. Directly produced spectra are shown by full lines while the reflected spectra are shown by dotted lines. The thick black line corresponds to the spectrum at the peak of the directly produced luminosity – see Fig.2.

(ii) The Saturation/Decay Phase

The description given above concerns the early phases of the pair/photon growth before their number has been built substantially inside the system. When this eventually happens there are two competing effects which become dominant.

a) The relativistic protons become increasingly shielded by the produced electron/positron

pairs, with the reflected photons having an increasing probability of undergoing Compton scattering instead of a pair-producing Bethe-Heitler collision. We note that the rate of the latter reaction for a stationary proton distribution is proportional to $\mathcal{R}_{BH} \propto n_{\mathrm{p}} n_{\gamma} \propto e^{st}$, while the rate of the former is $\mathcal{R}_{ics} \propto n_e n_{\gamma} \propto e^{2st}$. Even if we were to assume that protons do not lose energy, this effect alone would eventually lead to saturation of the instability.

b) The increasing number of photons above the critical frequency of the PPSR loop and the ensuing production of pairs at the expense of the proton energy leads to proton "cooling". Thus, while the total proton number does not change, their maximum energy decreases below the threshold energy necessary for the loop to operate. As a result, no new pairs are injected into the plasma which evolves by the cooling of the pairs already present and the decrease of its luminosity.

In reality both effects take place simultaneously. However, if the loop operates close to threshold, the proton losses are rather slow and the luminosity decreases at a correspondingly slow rate. On the other hand, operation of the loop well inside the unstable regime will lead to much faster proton losses and consequently faster photon cooling.

Figure 2 depicts the evolution of the photon compactness (both directly produced and reflected) as measured in the RBW frame once in Zone II. We note that initially the photons grow with an index $s = 5.1$ up to the point that $\ell_{\gamma}^{R} > \ell_{\mathrm{b}}$. At this point the dominant electron cooling process shifts from synchrotron to inverse Compton and as a result the growth rate changes. The photon density of the system saturates once it reaches a sufficiently high level due to the combination of the proton energy losses that prevent further pair production and Compton saturation – see above. In the particular example protons lose about 1.5% of their energy which is turned into radiation. As we will see in the next section, depending on the initial parameters, protons can lose a substantial portion of their energy.

An important quantity in our analysis is the number density of cooled pairs. These are the pairs that are produced by the Bethe-Heitler pair production process, initially at Lorentz factors $\gamma = \Gamma$, and have subsequently cooled down to $\gamma \simeq 1$ by synchrotron and inverse Compton losses. The code described in Section 3 follows both the production and evolution of these particles and thus it can provide at each instant the quantity $n_e^{cool}(t)$ which, using the normalizations of Section 3.1, is equal to $\tau_T(t)$. As it can be seen from Fig. 2 their density builds quickly during the growth phase and after the onset of the saturation/loss phase it remains almost constant in the system. We also note that $\tau_T(t) \ll 1$, i.e. in our model (and for the chosen values of the parameters) the RBW continues to be optically thin throughout the burst and hence its directly produced spectrum is not modified by repeated Compton scatterings. This is different from the results of MPK05 who investigated the properties of the PPS loop in the absence of reflection. The reason for this difference, as we

have emphasized in Section 2, is the presence of upstream reflection which greatly relaxes the threshold criteria and as a result both the required initial proton number density and the number of the produced pairs decrease.
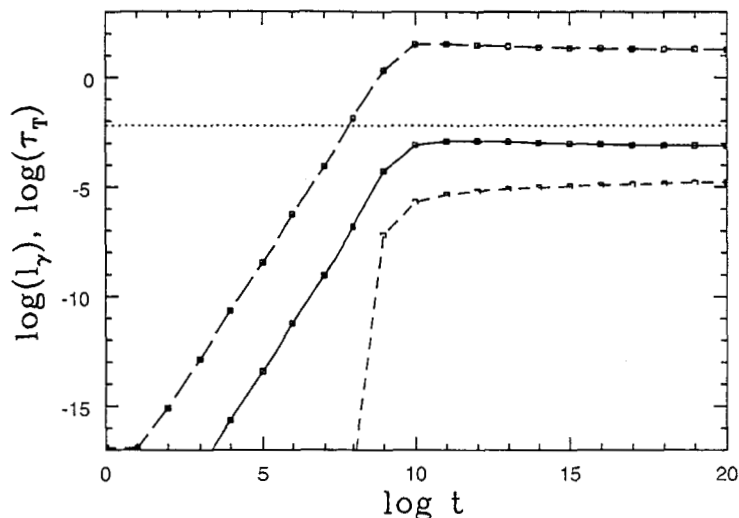

Fig. 2.— Lightcurves of the directly produced photon compactness (full line), reflected photon compactness (long dashed line) and number density of cool pairs (normalised here to the Thomson optical depth – short dashed line) as measured from the time the RBW has entered the reflection zone for the parameters of the previous figure. Time is measured in blob crossing times. The horizontal dotted line denotes the magnetic compactness

(iii) The Observed Spectrum

The processes described in the above subsections refer to quantities (electron and photon densities) as measured in the RBW frame. An observer at Earth will observe the two spectral components (synchrotron and inverse Compton) shifted by δ in energy and by δ^3 in flux (in the case of a spherically symmetric expansion we can simply set $\delta = \Gamma$). This observer will not see the reflected component as this is directed away from him/her. However, any

reflected photon which is scattered on the cooled pairs of the RBW will be isotropized in the frame of the flow and, upon transformation to the observer's frame, it will appear beamed within a cone of opening angle $\simeq 1/\Gamma$, just like the SSC components with the same flux amplification ($\propto \delta^3$). Thus the observed spectrum will have a third component, which we shall refer to as the "doubly reflected" component and which is of special interest in our model as its peak emission lies in the 0.5 to 10 MeV regime for a wide set of parameters – more details will be given in the next section.

The most conservative case concerning the flux of this "doubly reflected" component is that in which there are initially no "cold" pairs in the RBW; however, as the PPSR loop begins to operate, an increasing number of them accummulates near $\gamma \simeq 1$ (see Fig. 2) by the cooling of those produced by the Bethe-Heitler process. Thus the relative importance of the doubly reflected component to the directly produced synchrotron one will depend solely on τ_T – note that only the synchrotron component, which can be a small fraction of the total internal luminosity, will be effectively scattered by the mirror.

Figure 3 shows the multiwavelength spectrum at the instant when the internal luminosity peaks. The doubly reflected component (dotted line) peaks in this case at about $5\,(\delta/400)$ MeV, while the directly produced synchrotron and inverse Compton components peak respectively at $E_\mathrm{s} \simeq 30(\delta/400)$ eV and $E_\mathrm{ic} \simeq \delta\Gamma\, m_e c^2 \simeq 80(\delta/400)$ GeV.

5.   Modeling the PPS Network – Including the Effects of Electrons

In the previous section we outlined the basic ideas of the Pair Production/Synchrotron loop in the presence of reflection (PPSR) emphasizing the fact that the growth of pairs and photons can take place in the presence of protons alone, i.e. without any need for an initial photon or electron populations. In this section we use less restrictive, more realistic assumptions by including in our calculations an initial population of electrons, an assumption we retain for the rest of the paper. Since the plasma must be neutral, the least contrived assumption is that the number density of initial electrons equals that of the protons (one could also assume the additional presence of several e^+e^- pairs per electron but we will refrain from doing that at present). We also note that the energy of these electrons as the RBW enters the reflection zone (where all the action takes place) is essentially a free parameter. The electrons are considered to be a part of the flow of the RBW and therefore the randomization of their energy is expected to bring them to Lorentz factors $\gamma_e = \gamma_p = \Gamma$. However, with cooling times far shorter than those of protons, they begin cooling immediately upon their injection into the RBW; by the time the RBW achieves its terminal Lorentz factor Γ the electrons may have attained various degrees of cooling and this might occur well before
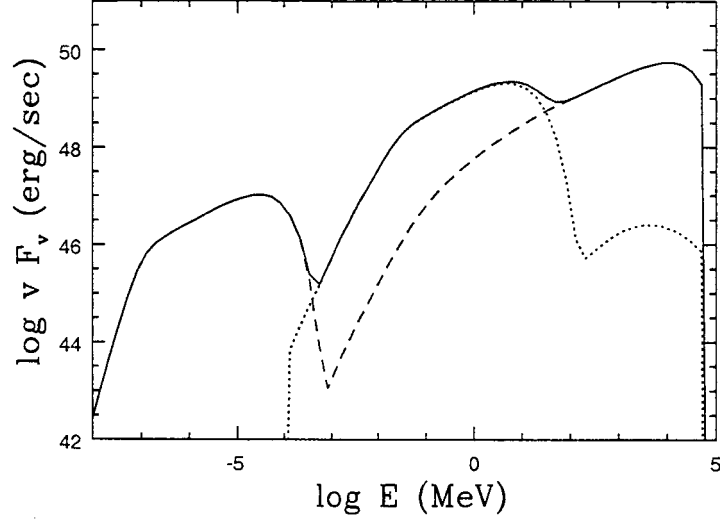
Fig. 3.— Snapshot of the multiwavelength spectrum at the peak of the direct emission as seen by an observer at Earth in the case of the parameters of Fig. 1 and for $\delta = \Gamma$. The dashed line corresponds to the directly produced component while the dotted line to the doubly reflected component. The full line is the composite spectrum.

the RBW has reached the assumed reflection zone. Because the evolution of our model is determined by the number of photons available in the system, the presence or not of electrons that can readily produce such photons is expected to influence the solution of the PDEs (8) to (10).

In order to avoid introducing an additional set of free parameters pertaining to the maximum energy and normalization of the electrons, we study the evolution of the system in two extreme cases:

(i) The electrons have totally cooled upon entering the reflection zone. Thus we will assume that $n_p = n_e$ while $\gamma_p = \Gamma$ and $\gamma_e = 1$, and that the photons produced in the cooling
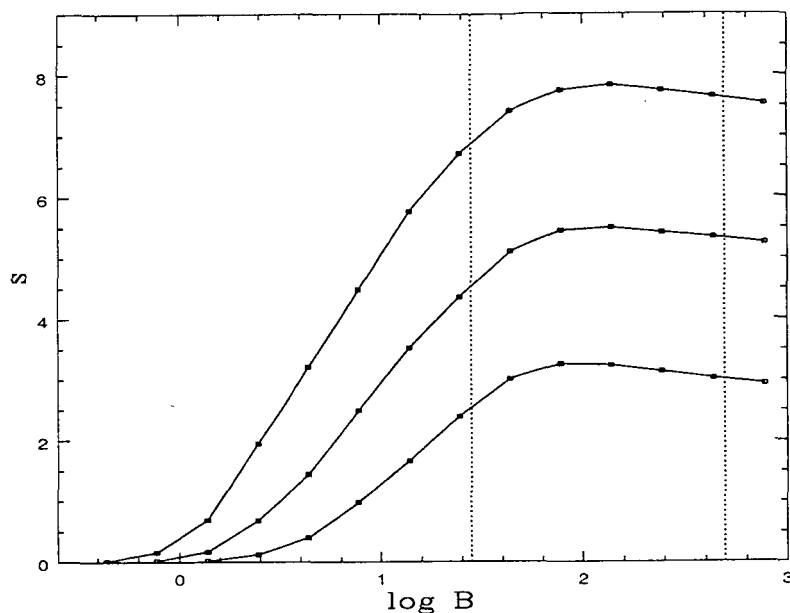
Fig. 4.— Plot of the photon growth index s versus the magnetic field strength B (in Gauss) for various values of the proton number density. The curves from left to right are for $n_p \tau_{\mathrm{mir}} = 10^5$, 10^4 and 10^3 cm^{-3}. The rest of the parameters are the same as those of the previous Figures. The vertical dotted lines represent the two magnetic fields that correspond to the synchrotron electron cooling time being equal to one crossing time for $\gamma = \Gamma$ (left curve) and $\gamma = 1.26 = \gamma_{min}$

process do not interact with the "mirror". This case, which we will call the 'Cooled Electron' (CE) case, uses identical assumptions to the ones of the example studied in the previous (no electron) section, with the only difference being the presence of a minimum value for τ_T related to the presence of this initial electron population.

(ii) The electrons have the same Lorentz factor as the protons upon entering the reflection zone. This would correspond to the case in which the RBW "sweeps" the material between the "inner engine" and the "mirror" which now forms part of the RBW. The fact that the electrons may have cooled in the meantime is actually of little importance. What really matters is the number of electrons swept and the photons that will result from their cooling. Because of the relativistic speed of the RBW, these photons are not really lost but they are just a distance R/Γ^2 ahead of the RBW, which can catch up with them once they scatter in the "mirror". In this case we simply let the electrons cool only after the RBW has reached close to the "mirror". We note that even under this assumption the bulk of the

energy of the RBW continues to be stored in protons as $U_p/U_e = m_p/m_e$, where U_p and U_e are, respectively, the proton and electron total energy content. We will call this case as the 'Energetic Electron' (EE) case.

The cases where the electrons cool in various degrees between the site the blob first reaches the Lorentz factor Γ and the starting point of the reflection zone can be considered as intermediate cases.

We have ran the code for various combinations of the values of the comoving magnetic field strength B, the number density of the protons and electrons and of the scattering depth of the mirror while keeping the rest of the parameters at their values of the previous section. Our objective is to study the effects of electron inclusion on the kinematic and dynamic thresholds as well as the energetics and spectral shape of the produced outburst.

As a first step we examine the rate of growth, s, in the CE case. This will help us determine the regime in the parameter space where the instability operates efficiently. A first important result is that the rate of growth remains the same for various combinations of n_p and τ_{mir} as long as their product is constant. Therefore we examine the behaviour of s for various combinations of the parameters B and $n_p\tau_{mir}$; the results are shown in Figure 4. We find that the loop cannot operate for sufficiently low values of the magnetic field strength B, a fact that is in quantitative agreement with the discussion given in Section 2. However we find that the threshold value (corresponding to $s = 0$) is not totally independent of the product $n_p\tau_{mir}$; this can be accounted by the fact that we use the full single electron synchrotron emissivity rather than its delta function approximation used in KM92 and KGM. We find also that the value of B_{min} is lower from the theoretically found value in KGM because the reflected photons are boosted not simply by Γ^2 but by $4\Gamma^2$ relaxing even more the threshold requirement.

The EE case, because of its very fast development - the presence of energetic electrons causes the protons to lose their energy in one or two crossing times, see Fig. 6 - and our finite time resolution, does not allow for a similar s $vs.$ B plot. As we will show later, in this case there are more meaningful ways to check the strength of the instability.

5.1.   Thresholds

In this section we expand on the results of Fig. 4 by investigating the full behavior of the photon growth in time. A study of their growth for various values of the comoving magnetic field provides insights on the kinematic threshold, while a similar study by varying the proton number density provides insights on the effects of the numerically derived dynamic

threshold.

(i) The Kinematic Threshold

Figures 5 and 6 show the photon lightcurves produced after the RBW has entered the reflection zone as measured in the comoving frame for various values of the RBW magnetic field. Both the proton and the electron number densities have been kept constant for all runs at $n_p = n_e = 10^4 \, \text{cm}^{-3}$ while $\tau_{\text{mir}} = 1$. Fig. 5 shows the case where all electrons have cooled completely when the RBW is still in Zone I (CE case) while the protons have initial energy $\gamma_{\text{p}} = \Gamma = 10^{2.6}$. Fig. 6 assumes that both species are initially at energy $\gamma_{\text{p}} = \gamma_{\text{e}} = \Gamma = 10^{2.6}$ (EE case). The B-field ranges from 0.12 to 120 Gauss with increments by a factor of 10 while the rest of the parameters are the same as those assumed in the example of section 4.

In the CE case (Fig. 5) the photons increase initially as $l_\gamma \propto e^{st}$ with s a function of the magnetic field strength B (see Fig. 4). At some point they reach saturation for the reasons explained in the previous section. As expected, for low enough values of B (rightmost curve) the increase is very gradual. For even lower B−values the photons do not grow at all in agreement with the kinematic threshold concept discussed in Section 2.

The case where the electrons are energetic (EE) before entering the reflection region (Fig. 6) exhibits some differences from the CE one. At low B−fields we get only the effects of the fast cooling electron population with the protons remaining practically unaffected. As the electrons cool very quickly on their own reflected radiation, the lightcurves peak equally fast (i.e. within one or two crossing times) after the entrance of the RBW inside the reflection zone. As the value of B increases the PPSR loop begins to operate and an increasing fraction of the proton energy is turned into radiation, as is manifested by the the higher peak luminosities and the longer decay times of the lightcurves.

These results are summarized in Fig. 7 that depicts the total photon energy radiated in each run as it is measured in the frame of the RBW. As we have already mentioned, the energy lost by the protons goes into electron-positron pairs and eventually escapes the system as radiation. Therefore, as the numerical code discussed in Section 3 conserves energy we expect

$$\int dt L_\gamma(t) = \Delta U_p + \Delta U_{e,in}, \tag{21}$$

where ΔU_p and $\Delta U_{e,in}$ is the total energy lost by the protons and initial electrons respectively and L_γ is the radiated photon luminosity. In practice, since the code calculates the photon luminosity at each crossing time t_i, the integral in the last relation has to be replaced by a sum of $\Sigma L_\gamma(t_i) \Delta t_i$.

The dashed and full lines in Fig. 7 represent the CE and EE cases, calculated from

Fig. 5 and 6 respectively. At low B there is a marked difference between the two cases: In the EE case, a substantial fraction of the initial electron energy is radiated, despite the fact that the system is below the PPSR threshold. For this reason we get essentially no radiation in the CE case that lacks the energetic electrons. As B increases the PPSR loop begins to operate extracting energy from the protons. We note that in the EE case, the presence of the initial energetic electron population (and the photons resulting from their cooling) allows the extraction of energy from the protons for lower values of the magnetic field. At even higher values of B both cases saturate at the same value of luminosity as the PPSR loop is capable of cooling the protons completely irrespective of the presence of initial energetic electrons – note however that, according to Figs 5 and 6, the resulting lightcurves are different as the time evolution of the system is sensitive to the initial conditions (i.e. the presence or not of relativistic electrons). In this respect, it is of interest to note that the present model allows for different characteristics of the GRB light curves on the basis of the values of its internal parameters. This is a desirable state of affairs as the light curve properties themselves could be used, in principle, to infer or restrict the values of these parameters.

(ii) The Dynamic Threshold

To study the dynamical criterion we performed runs keeping the strength of the co-moving field constant while varying the proton (and electron) number density. We show the results in Fig. 8. Here we show the fraction of energy that the protons lose during the outburst as a function of $n_{\rm p}$. We find that as $n_{\rm p}$ increases the outburst is able to extract an increasing fraction of the proton energy content. However the effects are less dramatic than in the previous case: changing $n_{\rm p}$ has an immediate effect on the efficiency of the PPSR loop but not on its existence. The loop operates in both the CE and EE cases with the EE case again being more efficient in extracting energy off the protons. Eventually the two cases converge at sufficiently large values of $n_{\rm p}$ and their efficiency in transfering energy from the protons approaches 100 %. It is worth mentioning at this point that all the above runs exhibit very similar synchrotron spectra, i.e. they all peak at the same energy, as the magnetic field has been assumed constant.

5.2. The Observed Spectra: Direct and Reflected Components

We proceed by studying the characteristics of the produced spectrum, both in the RBW frame as well as observed on Earth.

We find that in all cases the multiwavelength spectra produced on the RBW frame consist of a synchrotron component at low energies and an inverse Compton component at
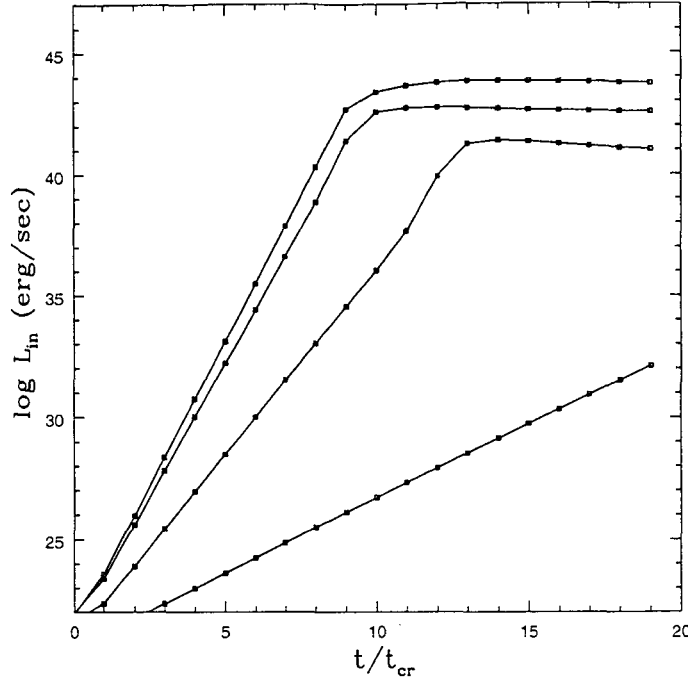
Fig. 5.— Plot of the photon luminosity evolution as this is measured in the comoving frame in the CE case where $n_p = n_e = 10^4\,\text{cm}^{-3}$ while the value of B has been assumed 4.4, 14, 44 and 140 Gauss (bottom to top). The rest of the parameters are as stated in the text. Time is measured in blob crossing times and the value $t = 0$ has been set at the instant when the RBW enters the reflection zone.

high energies. The spectra as observed on Earth have a third component that is produced from the double reflection of the aforementioned synchrotron component first on the mirror and then on the cooled pairs of the RBW (see Fig.3). Next we discuss the characteristics of each component separately.

(i) The Synchrotron Component

Once a value for Γ has been assumed, the only important parameter for determining the peak of the directly produced synchrotron spectra, at least during the growth phase, is the value of the comoving magnetic field B. The peak of the synchrotron component as observed in the RBW is given by $\epsilon_{s,p}^{RBW} = b\Gamma^2$ and thus the same quantity as observed at Earth is $\epsilon_{s,p}^{obs} = \delta b\Gamma^2$ (all energies are expressed in units of $m_e c^2$; in the above expressions and those of the next two subsections the superscript refers to the frame at which each energy is observed, while the subscript to the specific process considered with the p after the comma
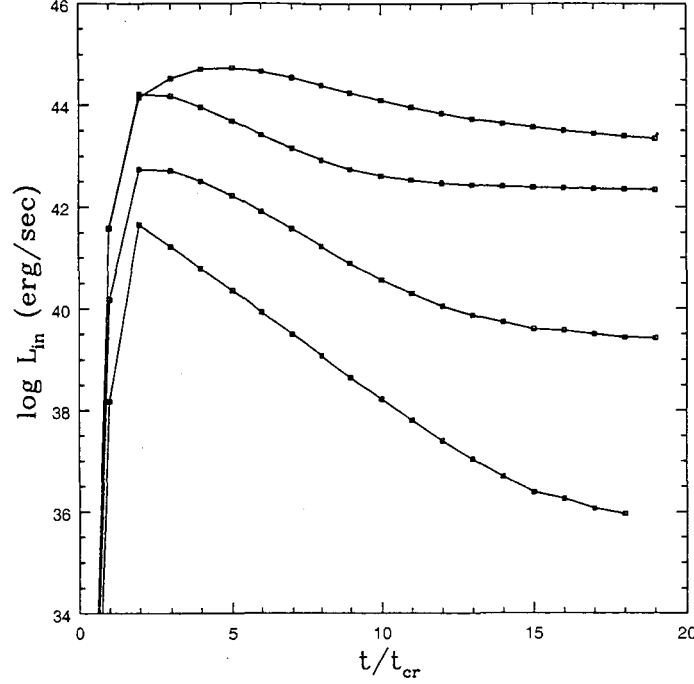
Fig. 6.— Plot of the photon luminosity evolution as this is measured in the comoving frame in the EE case where $n_p = n_e = 10^4 \, \mathrm{cm}^{-3}$ while B varies (bottom to top) from 0.12 G to 120 G by increments of a factor of 10. The rest of the parameters are as stated in the text. Time is measured in blob crossing times and the value $t = 0$ has been set at the instant when the RBW enters the reflection zone.

referring to the energy of peak emission of the specific process). One should note here the difference of our model from those more common in the literature for which the electron maximum energy is estimated from equipartition with protons arguments, yielding much higher energies for the electrons and synchrotron emission.

(ii) The Inverse Compton Component

The peak of the inverse Compton component is largely independent of the magnetic field strength B, as a substantial fraction of the relativistic electron collisions with the reflected photons (the dominant contributors to their losses) occur in the Klein-Nishina regime. Thus we expect the scattered photons to take a substantial fraction of the electron energy (Blumenthal & Gould 1971), leading to $\epsilon_{ICS,p}^{RBW} = \eta\Gamma$ and $\epsilon_{ICS,p}^{obs} = \eta\delta\Gamma$ with $0.1 < \eta < 1$.
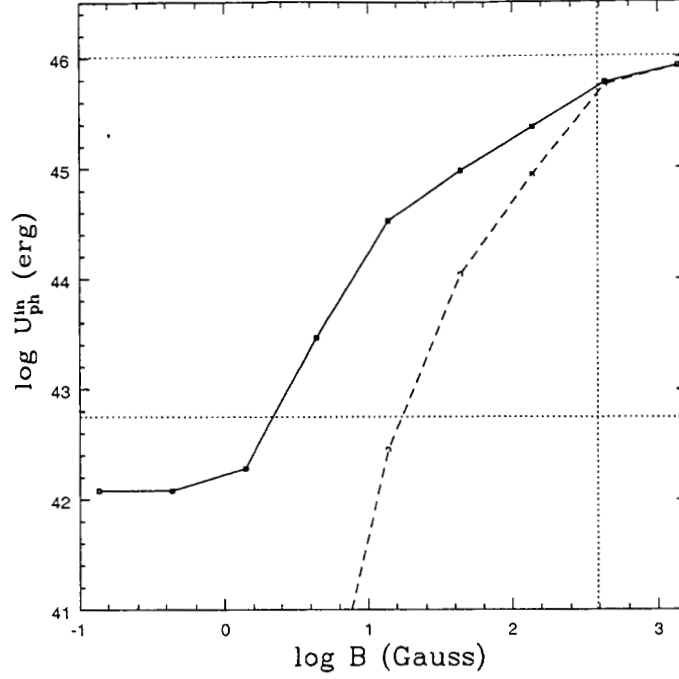
(iii) The Doubly Reflected Component

Fig. 7.— The total energy radiated by the protons in the case where $n_p = n_e = 10^4 \, \mathrm{cm}^{-3}$ as a function of the magnetic field strength B - both quantities are measured in the comoving frame. The other parameters are given in the text. Full and dashed lines represent the EE and CE cases respectively. The lower horizontal dotted line is the total energy content stored in electrons while the upper one is the energy stored in protons. The vertical dotted line is the equipartition magnetic field.

This component peaks around $\epsilon_{R,p}^{obs} \simeq \delta\Gamma^2 \epsilon_{s,p}^{RBW}$ where the factor δ comes from the Doppler blueshift and the factor Γ^2 comes from the reflection on the mirror. Using the value of $\epsilon_{s,p}^{RBW}$ given above, we arrive at $\epsilon_{R,p}^{obs} = \delta b \Gamma^4$ which is basically the relation derived in KGM (for $\delta = \Gamma$). As a matter of fact, since higher values of B produce higher synchrotron peaks we expect that Klein-Nishina corrections will modify the peak of the reflected spectra, therefore the analytic relation given above can be used as an upper limit.

Fig. 9 summarizes these results. It shows the peak energy of the three components as observed on Earth in the case where $\delta = \Gamma$ versus the comoving magnetic field strength. We notice that the synchrotron peak increases linearly with B, while the inverse Compton peak is largely independent of it and roughly equal to $\delta \Gamma m_e c^2$ i.e. maximum electron energy as preceived in the lab frame. The doubly reflected peak increases with B (as the PPSR loop
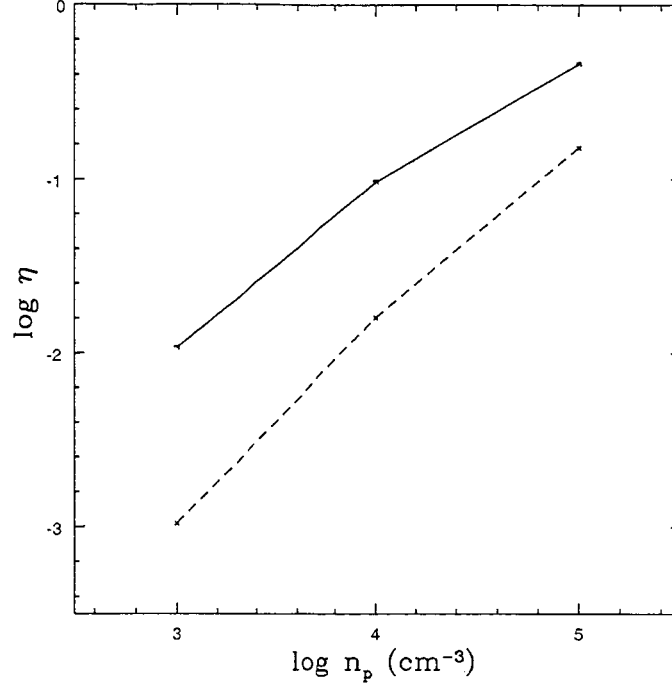
Fig. 8.— Fraction η of the proton energy content lost to radiation in an outburst as a function of the initial proton number density. The magnetic field has been assumed to be B=120 G. The full line curve corresponds to the EE case while the dashed line curve to the CE case. For the other parameters see text.

runs increasingly above its kinematic threshold) but the relation is slower than linear. Note that for combinations of Γ (here taken to be equal to 400) and B that are close to threshold (Eq. 3), this peak lies between the 100 keV - 1 MeV range, and as we emphasized in section 2 this is independent of the particular choice of Γ and B.

However we note that in reality the picture is much more complex. There is continuous evolution of the spectra due to the time-dependent cooling of electrons and protons and we find that as a result the frequencies of the peak emission of these components depend on time. Fig. 10 depicts the peak of the doubly reflected component as a function of the luminosity at each crossing time during the growth phase for various values of the comoving magnetic field. It is clear that we cannot attribute a unique value of the peak energy to a certain assumed value of the magnetic field. However, in order to simpilfy the picture, we can assign as a characteristic energy of the peak the energy during the growth phase and this is what is shown in Fig. 9.
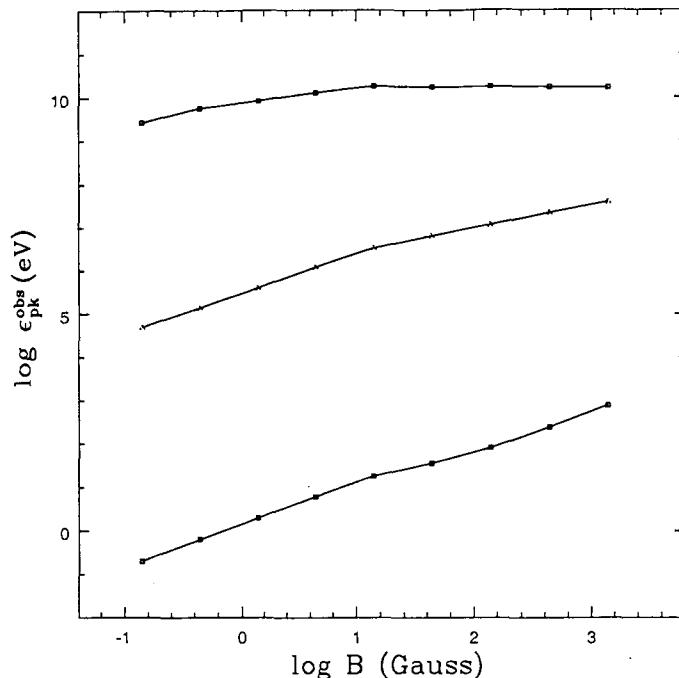
Fig. 9.— Plot of the peak of the observed synchrotron (lower curve), doubly reflected (middle) and inverse Compton (top) component versus the comoving magnetic field strength. For the parameters used see text

In addition to the energy of peak emission of the three components of the spectrum, we are also interested in their inferred total energy content, assuming their emission to be isotropic, a quantity found to exhibit several rather tight correlations in GRB statistics (e.g. Amati et al. 2002). In Section 5.1 we showed the dependence of the total radiated energy (as measured in the comoving frame) on the two important parameters of our problem, namely the comoving magnetic field strength and the number density of the particles. We find that during the peak of the burst the relation $\ell_b/\ell_\gamma^R \ll 1$ is true and therefore the bulk of the radiated electron energy will be emitted by the inverse Compton component, with only a small fraction of it radiated by synchrotron. This can be seen also from the test case of the previous section (Fig. 3).

However, the luminosity of the doubly reflected component has a different time dependence from the luminosity of the directly observed components shown in Fig. 6, as it depends (i) on the synchrotron luminosity of the direct component and (ii) on the number of cool pairs that have been accumulated during the outburst in the RBW, i.e. on the front's ability
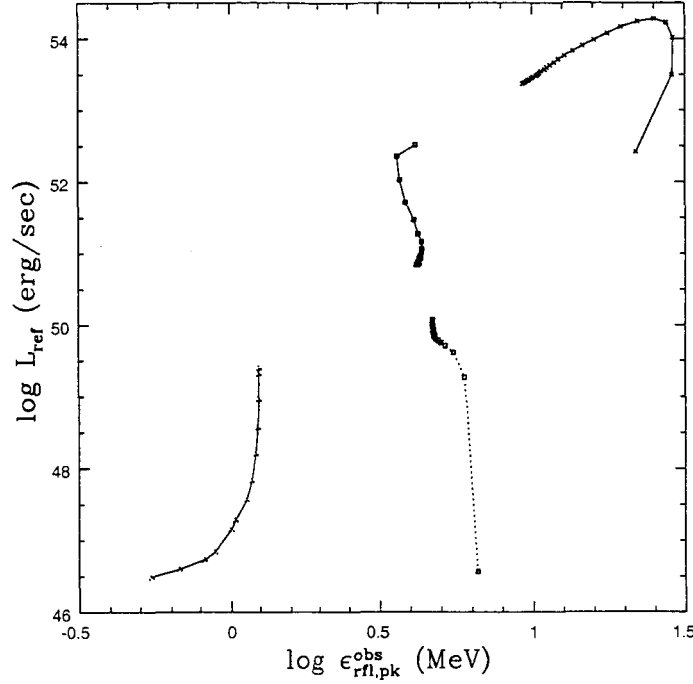
Fig. 10.— Plot of the evolution of the peak of the doubly reflected component versus the observed luminosity in that component in the EE case and for various comoving magnetic fields strengths. Left curve is for B=4.4 G, middle for B=44 G and right for B=440 G. For comparison the curve in the CE case for B=44 G has also been plotted (dotted line). Ticks represent the crossing times.

to scatter towards our direction at least a part of the reflected by the mirror radiation.

Fig. 11 depicts the total isotropic energy content of each of the burst components, i.e. the synchrotron, the IC, and the doubly reflected synchrotron as inferred by an observer on Earth as a function of the comoving magnetic field strength for the fiducial values of the rest parameters of our model. The solid line is the total directly radiated energy, which for all practical purposes can be considered equal to the energy radiated in the inverse Compton component; the dashed line is the energy radiated by the synchrotron component, while the dotted line is the inferred energy associated with the doubly reflected component at energy ~ 1 MeV and it is by and large the component that defines a GRB as such. The fast increase of this latter component with B is due to the increasing number of pairs produced in the RBW which, in turn, increase its scattering efficiency.

It is of interest to note that for sufficiently small values of B the energy in the reflected

component becomes comparable (or even less) to that of the synchrotron. As of today, there have not been any bursts exhibiting prompt optical isotropic energy (or, almost equivalently, flux) comparable to that of the γ-rays. In the context of the present model this constraint sets a lower limit on the value of the comoving field B. However, besides its dependence on B the ratio of these two components depends also on the value of n_p. While an increase in n_p leads to an overall higher photon production rate, it also leads to an increase in τ_T which amplifies only the luminosity of the scattered component.
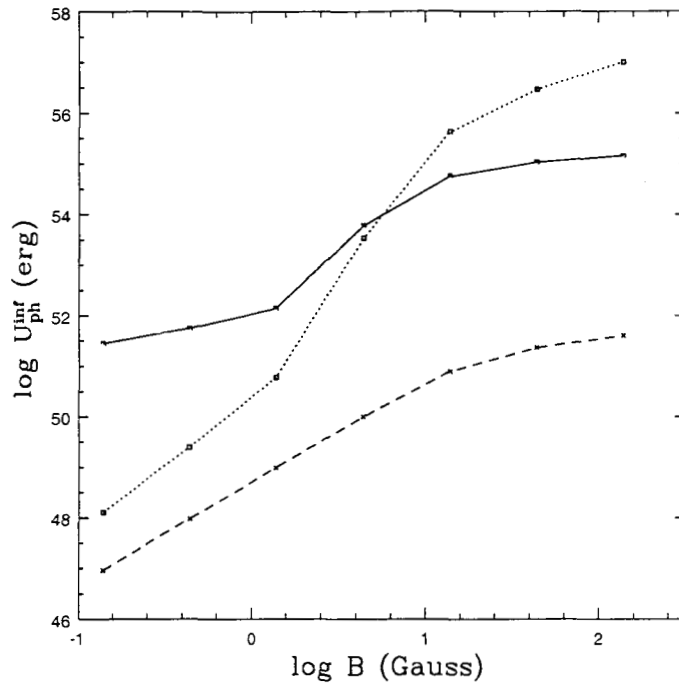

Fig. 11.— Plot of the 4π inferred energy content in an outburst versus the comovng magnetic field for the EE case. The full line curve corresponds to the total directly produced energy, the dashed line curve corresponds to the energy content in the synchrotron component while the dotted line curve to the energy content in the doubly reflected component. The particle number density is $n_p = n_e = 10^5\,\mathrm{cm}^{-3}$. For the rest of the parameters see text.

Fig. 12 exhibits the isotropic energy content in the doubly reflected component as a function of the energy of its peak emission (assuming $\delta = \Gamma = 400$ and the redshift of the burst $z_{GRB} = 0$) for various values of the proton number density of the RBW ($n_p = 10^3,\ 10^4,\ 10^5\,\mathrm{cm}^{-3}$, bottom to top) – and having in mind the possible complications introduced by the evolution as these were discussed in connection to Fig. 10. The figure shows that the energy of this component is a very strong function of $\epsilon_{R,p}^{obs}$ – for instance,

while $\epsilon^{obs}_{R,p}$ varies by two orders of magnitude, the energy varies by about nine. This strong dependence, in the presence of a flux limited sample results in a peak emission that occurs at approximately the same energy, largely independent of the total (inferred) energy of the GRB (provided that the observer is located close to the direction of motion of the RBW). One should note that this figure is precisely the so-called Amati relation (Amati et al. 2002) with the axes interchanged. The relation found by those authors is actually much weaker (its equivalent slope is 2 instead of 4.5 obtained here). With the discovery of the much less luminous X-Ray Flashes (XRF), it has been suggested (Lamb et al. 2004) that the Amati relation extends to much lower energies and encompasses both classes of transients. The physics behind such a unification between GRB and XRF is currently uncertain; however, Yamazaki et al. (2003) proposed that, similarly to AGN, the GRB – XRF unification is related to the orientation of the RBW velocity relative to the observer, with the XRF being GRB viewed at angles $\theta > 1/\Gamma$. The relation of figure 12 is an intrinsic one and not related to the orientation of the observer which is set to $\theta = 1/\Gamma$.
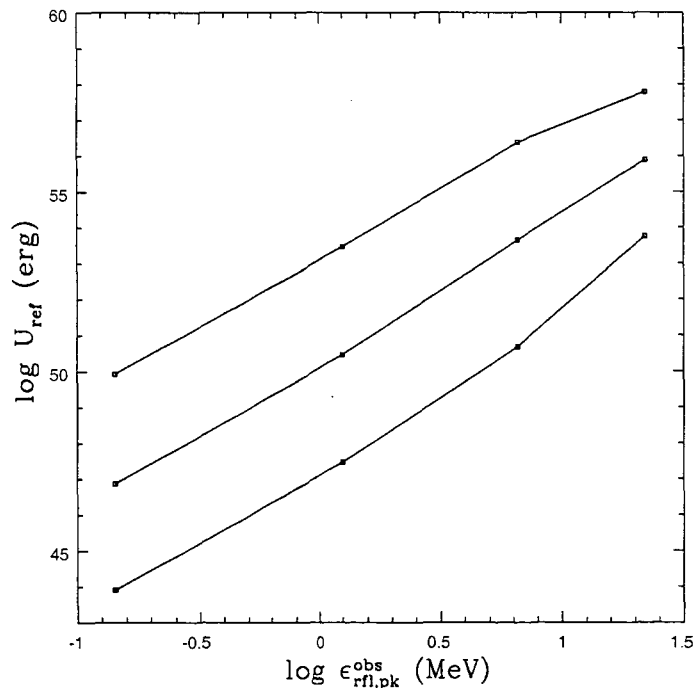

Fig. 12.— Plot of the isotropic energy content of the reflected component as inferred at Earth versus the peak of its emission (assuming $\delta = \Gamma = 400$) for various values of the proton number density ($n_p = 10^3$, 10^4, $10^5\,\mathrm{cm}^{-3}$, bottom to top).

6. Summary, Discussion

In the present paper we have simulated in considerable detail the spectral and timing properties of GRB emission within the framework of the "Supercritical Pile" model proposed earlier by KGM. This model was conceived as a means of resolving two fundamental problems of GRB, namely the dissipation and conversion into radiation of the energy stored in the protons of the RBW of a GRB and the narrow distribution in the energy of the GRB peak emission E_p. The "Supercritical Pile" model resolves both issues with a single set of assumptions, making it in this respect unique among GRB models. As discussed in KGM, the fundamental process behind the dissipation of the proton energy is the radiative instability discussed in KM92 and MK95, enlarged in scope to include the reflection of photons by matter upstream of the advancing RBW, a modification that helps reduce the kinematic and dynamic thresholds. Both ingredients are important in producing model spectra in general agreement with observations and model parameters consistent with those thought to prevail in GRB.

The detailed calculations of the present paper show that: (i) The presence of reflection reduces both the kinematic and dynamic thresholds of the PPSR loop discussed by KM92 in accordance with the arguments put forward in KGM. (ii) The process invoked in KGM can indeed extract a substantial fraction of the proton energy within a few crossing times of the radiating segment of the RBW, for judicious choices of the model parameters; for typical values of the Lorentz factor Γ, this time scale is in general agreement with GRB observations. (iii) The prompt νF_ν GRB spectrum comprises the following three components (in the observer's frame): (a) A broad feature with peak luminosity at energy $E_s \simeq m_e c^2/\Gamma^2$ i.e. at IR-optical-UV frequencies, the result of synchrotron radiation by the pairs produced by the instability. (b) A component with a peak at high energies ($E_\gamma \simeq \Gamma^2 m_e c^2$), produced by the inverse Compton scattering of the internally produced and reflected radiation on the 'hot' (i.e. uncooled) pairs of the RBW. (c) A component produced by the Compton scattering of the reflected radiation on the 'cool' pairs that have been accumulated on the RBW. This last component peaks in the range of $(0.5 - 10)\,\delta/\Gamma$ MeV (in the observer's frame), an energy which reflects the kinematic threshold of the loop and thus it is largely independent of the particular value of Γ.

The important parameters of our problem are the comoving magnetic field strength B, the proton number density in the RBW frame n_p, and the value of the bulk Lorentz factor Γ. Other parameters such as the optical depth of the "mirror" and the existence or not of energetic electrons are less crucial for the formation of the spectra, but of importance for the ensuing time evolution. An additional parameter which we believe it to be of great importance for the observed GRB spectra but which we have not explored at all as yet is

that of the angle between the velocity of the 'blob' and the observer's line of sight (see e.g. Ioka & Nakamura 2001) which has been proposed as the parameter leading to the unification between GRB and XRF (Yamazaki et al 2003). This parameter proliferation does not pose necessarily a problem for our (or for that matter any) model, since, as pointed out in a recent in-depth analysis of GRB light curve properties, at least five parameters are needed to model their diverse light curve properties (Norris et al. 2005). It is important to stress again here that despite the large number of available parameters the value of E_p is of rather limited range, in agreement with observations.

Our calculations have been done self-consistently by solving simultaneously the three space-averaged time-dependent kinetic equations for protons, electrons and photons, taking into account all relevant processes between the species and calculating exactly the reflected photon component entering at each instant the RBW. From all the relevant processes, the ones that play a key role are Bethe-Heitler pair production, while synchrotron radiation and inverse Compton scattering of electrons-positron pairs are also important during the early phases and saturation of the outgrowth respectively. The rest processes, while included in the code, are of marginal importance. Thus photon-photon pair production either does not apply (as is the case for collisions between the directly produced synchrotron photons and the reflected photons which do not meet the threshold requirement) or has a very low optical depth (as is the case for collisions between the directly produced photons of the inverse Compton component and the reflected component ones). Therefore, the implied modifications on the photon spectrum and on the pair production injection rate are very small and not able to alter any of our analytical (and numerically verified) results. Similarly we find that electron-positron annihilation is negligible as the pairs produced from thr Bethe-Heitler process never become optically thick, at least for the conditions considered herein. Finally, adiabatic losses have not been taken into account but as the whole burst episode requires only a few crossing times, this type of losses can be neglected.

A (perhaps significant) limitation of our calculations is the assumption of a constant bulk Lorentz factor Γ. This might have led to an overestimation of the burst luminosity, especially during its decay phase, as potentially important Compton drag effects and reduction in the value of Γ have not been taken into account. However this is not expected to alter our results during the growth and peak phases as the protons have not lost yet any substantial part of their energy so the evolution under a constant Γ appears to be a valid hypothesis. In this respect, we would like to point out that our model offers a natural explanation for the termination of the prompt phase of the GRB and the onset of the afterglow: this comes about when the values of Γ and/or B drop below the values need to fulfill the kinematic threshold of our model. At this point no more electron injection takes place and the GRB enters the afterglow phase characterized by the cooling of the available electron population.

We should point out for the benefit of the reader that in a realistic model, the RBW in its propagation sweeps new material lying ahead of it, thus increasing its column density. In our calculations we have ignored this additional increase in column density as well as the concommitant decrease in Γ.

There are several issues that we have not addressed or explored in our analysis, mainly because we would like to keep it focused on the issue of spectral formation and evolution but also of finite length. These include:

(1) The origin and dynamics of the "mirror": Our discussion to this point assumed that the "mirror" is static relative to the observer, a situation most appropriate, in our opinion, to the "external shock" GRB model. However, given the current interest in the alternative "internal" shock models, and also in the possibility that the GRB flux may impart a non-zero velocity on the mirror matter (Beloborodov 2002), it is easy to generalize our model to include the effects of the relative motion between the RBW and the "mirror". Such an arrangement will modify the kinematic threshold condition from $b\,\Gamma^5 \simeq 2$ to $b\,\Gamma^3\,\Gamma_{\rm rel}^2 \simeq 2$, where $\Gamma_{\rm rel}$ is the relative Lorentz factor between the RBW and the "mirror". Arguments very similar to those of Section 2 indicate then, that in this case the peak energy of the doubly scattered component will be at energy $E_{\rm p} \simeq b\,\Gamma^3\,\Gamma_{\rm rel}^2 \simeq 2$, i.e. it will remain unchanged (it reflects the threhold for pair production), as implied by observation. However, in this case the peak emission of the synchrotron and IC components will be at energies smaller and larger than $E_{\rm p}$ by a factor $\Gamma_{\rm rel}^2$ respectively rather than Γ^2. Of course, a small value for $\Gamma_{\rm rel}$ will have to be compensated by a correspondingly larger value for Γ in order to fulfill the kinematic threshold. Along the same lines of internal shock models, one might consider the case of a burst of finite duration in which the radiation from its earlier ejected segment that has slowed-down, serves as the source of photons in place of the radiation reflected on the "mirror". The evolution in such a case becomes more complicated because it depends on the details of the kinematics of the entire burst front structure. However, assuming that the emission from the slowed-down section is again at an energy roughly equal to $\epsilon_s \simeq b\Gamma^2$ leads to spectra very similar to those produced by our present calculations.

In our work so far we have refrained from discussing the nature of the "mirror" invoked in our model. As far as the kinematic threshold of our model is concerned, this is independent of the "mirror" albedo $\tau_{\rm mir}$. However, the dynamic threshold, and hence the efficiency of radiating away the proton energy, does depend on this parameter as indicated in Eq.(4). Assuming the same column density for the scattering in the "mirror" and using that the ratio of the Thomson to the $p\,\gamma$ reaction cross-section is about 300 (true for values of the collision energy about 10 times above threshold) we obtain from Eq. (4) the condition $\tau_{\rm mir} \gtrsim 4\,\Gamma^{-2}$ which is satisfied for $\Gamma \gtrsim 430$ when the density and radius are $n \simeq 10^3$ cm^{-3}

and $R_{16} = 3$ respectively. The condition on the density and radius are consistent with a wind of $\dot{M} \simeq 3 \times 10^{-6}$ $M_\odot \, yr^{-1}$ and velocity $v \simeq 10^8$ cm/s. At this point we would like to re-iterate that fulfilling only the kinematic (but not the dynamic) threshold would still result in a burst, however one which is rather inefficient in converting the proton energy into radiation. Finally, an intriguing possibility is the increase of the number of pairs ahead of the shock by the scattering of the high energy photons and their conversion into electron-positron pairs, as discussed by Beloborodov (2002), who indicates that, under certain circumstances, it may be possible to obtain a pair depth as high as $\simeq 1$.

(2) Exploring the B, Γ, n_p parameter space for correlations with GRB phenomenology: Our present models were all run with a given value of Γ. Our results indicate the time evolution to be faster for combinations of B, Γ well above the kinematic threshold; at the same time, however, the value of E_{p} is larger for such combinations, in agreement with the general observation that faster varying bursts are generally harder than slower varying ones. Lower values of Γ can be compensated by larger values of n_p, which however lead to different values of E_{iso} or peak luminosity.

Finally, we should re-iterate that, contrary to most, our model produces spectra in general agreement with observation without the need to invoke the presence of shock accelerated particle populations. The presence of such populations is not excluded, neither would invalidate any of the present results; however, it would lead to spectra more complicated than those produced in this paper that, in addition, extend to energies higher than those suggested in this work. One can argue by simple inspection of the threshold conditions (which can now be fulfilled for much lower values of Γ) that the presence of a non-thermal population of relativistic protons would result in emission of high energy radiation long after the prompt GRB emission at $\simeq 1$ MeV has died out. Apparently, there has been at least one such event so far, i.e. GRB 941017, registered in the NaI calorimetric detectors of EGRET aboard CGRO (González et al. 2003). It is also of interest to note that the highest photon associated with GRB emission came approximately 90 minutes after the end of the prompt emission in GRB 940217 (Hurley et al. 1994). The impending launch of GLAST with its superior sensitivity may lead to the discovery of more similar events, which will test the extension of the particle distributions in GRB to energies higher than considered in this note.

The model presented herein makes several concrete predictions. Thus we expect that, if the ~ 1 MeV GRB are produced in the way prescribed by this model, they should be accompanied by prompt emission in the IR-optical band (the synchrotron component of the direct emission), as well as in the GeV-TeV regime (inverse Compton component). The precise energies of the above peaks depend on Γ and the comoving magnetic field, however

the model predicts that GRB should be strong emitters at energies $\sim \Gamma^2$ (in $m_e c^2$ units). This is from the inverse Compton component which, during the peak of the burst, dominates the synchrotron component by many orders of magnitude. Thus GRB should be abundantly detected by both the GBM and the LAT instruments aboard GLAST, and possibly by ground based TeV telescopes.

To date there have been a couple of GRB with prompt optical emission. The first one was that of GRB 990123 detected by ROTSE, with optical luminosity $\simeq 10^{-3}$ of that of the γ–ray band detected by BATSE aboard CGRO. Based on the fact that its optical light curve did not follow the detailed shape of the BATSE one, it has been argued that emission in this band is due to synchrotron radiation by the reverse shock of the RBW (Sari & Piran 1999). Interestingly, synchrotron emission by this component scales $\propto \Gamma^2$ (see Piran 2004, Eq. (72)) just like the synchrotron emission of our model. The second burst with optical prompt emission was that of GRB 041219a, detected by *Swift* in γ–rays and by the RAPTOR ground based system (Vestrand et al. 2005) in the optical band. Contrary to the case of GRB 990123, the optical light curve of GRB 041219a did follow the details of the time evolution of its γ–ray light curve, in agreement with the tenets of the present model. It is also of interest to note, that in this case too the optical luminosity was roughly $\simeq 10^{-3}$ of the high energy one, while the extrapolation of its optical spectrum did not match that of the high energy one, suggesting two spectrally distinct components. The presence of *Swift* in orbit guarantees that there will be more GRB with prompt emission from IR - optical to X-rays to γ–ray that will help determine the viability or not of our model.

Also of interest are observations by INTEGRAL as the peak of the doubly reflected component occurs within the INTEGRAL observing energy band, a feature that can allow direct comparison between our model and observations. To conclude we only mention the possibility of neutrino emission within the present scenario. This would be possible if the Lorentz factor of the RBW were sufficiently high to lead to pion photo-production. This emission could be present both in the "prompt" GRB phase, produced as suggested above, or by an accelerated proton component after the end of the prompt phase, provided that the proton distribution extends to sufficiently large values that fulfill the kinematic threshold condition.

Finally, we would like to point attention to possible polarization signatures of the prompt GRB emission in the component comprising E_p within our model: Because within our model this component is due to Compton scattering (rather that synchrotron emission as in most models) it should be highly polarized (up to 100%) if, as believed, it represents emission viewed at angles $\theta \simeq 1/\Gamma$. The highly polarized emission of GRB 031206 detected by RHESSI (Coburn & Boggs 2003), while not totally conclusive adds one more piece of evidence

in agreement with the model presented above.

REFERENCES

Amati, L. et al. 2002, A&A, 390, 81

Band, D. et al. 1993, ApJ, 413, 281

Baring, M. & Harding, A. K. 1995, Adv. Space Research, 15, 153

Beloborodov, A. 2002, ApJ, 565, 808

Bloom, J. S., Frail, D. A. & Kulkarni, S. R. 2003, ApJ, 594, 674

Blumenthal, G. R. & Gould, R. J. 1970, Rev. Mod. Phys., 42, 237

Böttcher, M. & Dermer, C. D. 1998, ApJ, 501, L51

Coburn, W. & Boggs, S. E. 2003, Nature, 423, 415

Cohen,E., Katz, J. I., Piran, T., Sari, R., Preece, R. D. & Band, D. L., 1997, ApJ, 448, 330

Costa, E. et al. 1997, Nature, 387, 783

Fenimore, E. E., Epstein, R. I. & Ho, C. 1993, A&AS, 97, 59

Frail, D. A. et al. 2001, ApJ, 562, L55

Ghisellini, G., 2003, in "GRB in the Afterglow Era", PASP Conf. Series, Vol. 312, p. 319 (astro-ph/0301256)

González, M. M. et al. 2003, Nature, 424, 749

Hurley, K. et al. 1994, Nature, 372, 652

Ioka, K. & Nakamura, T. 2001, ApJ, 554, L163

Kazanas, D. & Mastichiadis, A., 1999, ApJ, 518, L17

Katz, J. I., 1976, ApJ, 206, 910

Katz, J. I., 1994, ApJ, 422, 248

Katz, J. I., 1994b, ApJ, 432, L107

Kazanas, D., Georganopoulos, M. & Mastichiadis, A. 2002, ApJ, 578, L15 (KGM)

Kirk, J. G. & Mastichiadis, A., 1992, Nature, 360, 135 (KM92)

Krolik, J. H. & Pier, E. A. 1991, ApJ, 373, 277

Lamb, D. Q., Donaghy, T. Q. & Graziani, C. 2004, New Astron. Rev. 48 459-464 (also astro-ph/0309456)

Lightman, A. P. 1981, ApJ, 244, 392

Mastichiadis, A. in 'Relativistic Flows in Astrophysics', edited by A.W. Guthmann, M. Georganopoulos, A. Marcowith and K. Manolakou. Lecture Notes in Physics, vol. 589, p.1

Mastichiadis, A. & Kirk, J. G., A&A, 295, 1995, 613 (MK95)

Mastichiadis, A., Protheroe, R. J. & Kirk, J. G. 2005, A&A, 433, 765 (MPK05)

Mallozzi, R. S. et al. 1995, ApJ, 454, 597

Motz, J.W., Olsen, H.A., & Koch, H.W. 1969, Rev.Mod.Phys., 41, 581

Norris, J. P., Bonnell, J. T., Kazanas, D., Scargle, J. D., Hakkila, J. & Giblin, T. W. 2005, ApJ (in press; astro-ph/0503383)

Paczyński, B. 1986, ApJ, 308, L43

Piran, T. 2004, Rev. Mod. Phys., 76, 1143

Preece, R. D., Briggs, M. S., Mallozzi, R. S. Pendelton, G. N. Paciesas, W. D. and Band, D. L. 2000, ApJS, 126, 19

Rees, M. J. & Mészáros, P., 1992, MNRAS, 258, L41

Salmonson, J. D. & Galama, T. J., ApJ, 569, 682

Sari, R. & Piran, T. 1999, ApJ, 517, L109

Shemi, & Piran, T. 1990, ApJ, 365, L55